Shie Qian and Dapang Chen

Understanding the

NATURE OF SIGNALS

Whose POWER SPECTRA

Change with Time.

Joint Analysis

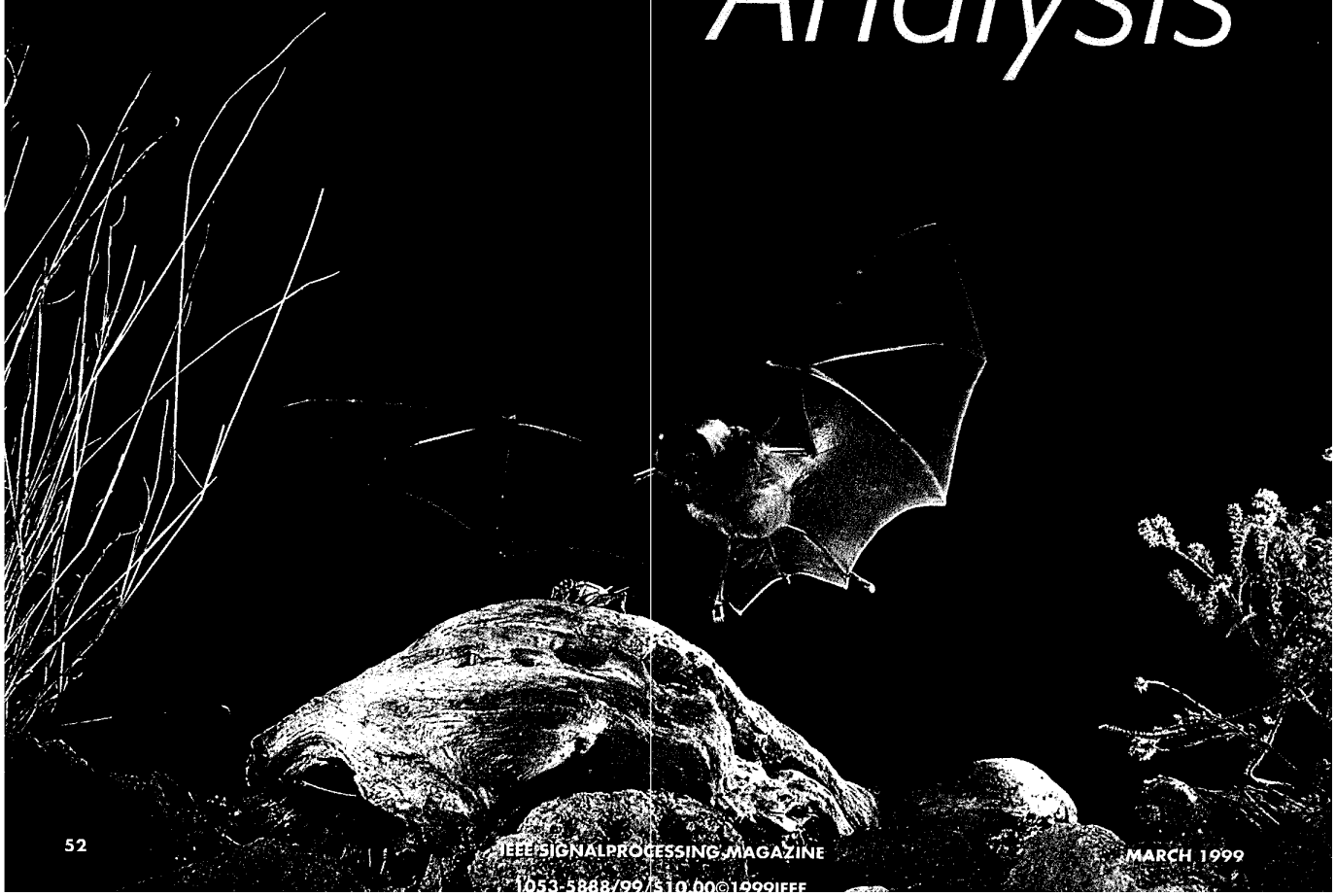

1053-5888/99/$10.00©1999IEEE

It has been well understood that a given signal can be represented in an infinite number of different ways. Different signal representations can be used for different applications. For example, signals obtained from most engineering applications are usually functions of time. But when studying or designing the system, we often like to study signals and systems in the frequency domain. This is because many important features of the signal or system are more easily characterized in the frequency domain than in the time domain.

Although the number of ways of describing a given signal are countless, the most important and fundamental variables in nature are *time* and *frequency*. While the time domain function indicates how a signal's amplitude changes over time, the frequency domain function tells how often such changes take place. The bridge between time and frequency is the *Fourier transform*.

The fundamental idea behind Fourier's original work was to decompose a signal as the sum of weighted sinusoidal functions. Despite their simple interpretation of pure frequencies, the Fourier transform is not always the best tool to analyze "real life signals," which are usually of finite, perhaps even relatively short duration. Common examples include biomedical signals [38], [50], [51], [53], [62] and seismic signals (Fig. 1). The seismic signals are not like the sinusoidal functions, extending from negative infinity to positive infinity in time. For such applications, the sinusoidal functions are not good models.

In addition to linear transformations, the square of the Fourier transform (power spectrum) is also widely used in many applications. However, the power spectrum in general is only suitable for those signals whose spectra do not change with time.

One common example is the speech signal. The bottom plot of Fig. 2 is the time waveform of the word "hood" spoken by a five-year-old boy. The plot on the right is the standard power spectrum, which reveals three frequency tones. From the spectrum alone, however, we cannot tell how those frequencies evolve over time. The larger plot in the upper left is the time-dependent spectrum, as a function of both time and frequency, which clearly indicates the pattern of the formants. From the time-dependent spectrum, not only can we see how the frequencies change, but we also can see the intensity of the frequencies as shown by the relative brightness levels of the plot. In other words, by analyzing the signal in time and frequency jointly, we are able to better understand the mechanism of human speech.

Although the frequency content of the majority of signals in the real world evolves over time, the classical power spectrum does not reveal such important information. In order to overcome this problem, many alternatives, such as the Gabor expansion, wavelets [21], and time-dependent spectra, have been developed and widely studied. In contrast to the classical time and frequency analysis, we name these new techniques as *joint time-frequency analysis*.

In this article, we introduce the basic concepts and well-tested algorithms for joint time-frequency analysis. Analogous to the classical Fourier analysis, we roughly partition this article into two parts: the linear (e.g., short-time Fourier transform, Gabor expansion) and the quadratic transforms (e.g., Wigner-Ville distribution). Finally, we briefly introduce the so-called model-based (or parametric) time-frequency analysis method.

Expansion and Inner Product

In what follows, we will first review the fundamental mathematical tools to perform the joint time-frequency analysis, that is, signal expansion and inner product. As we all understand, for a given signal s from the domain Ψ, where Ψ can be of finite dimension or infinite dimension, we may write a signal s in terms of a linear combination of the set of elementary functions $\{\psi_n\}_{n\in Z}$, where Z denotes the set of integers for the Ψ domain, i.e.,

$$s=\sum_{n\in Z} a_n \psi_n \tag{1}$$

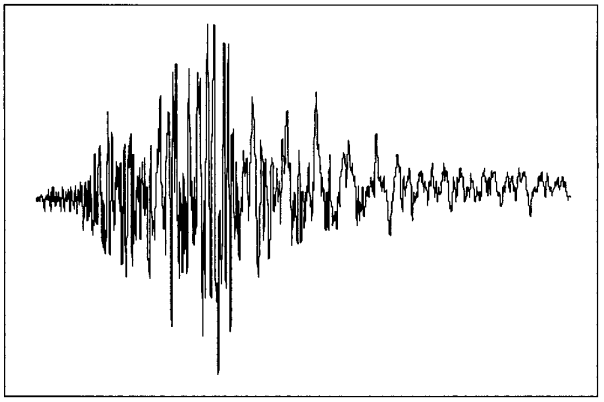

▲ 1. Seismic signal.

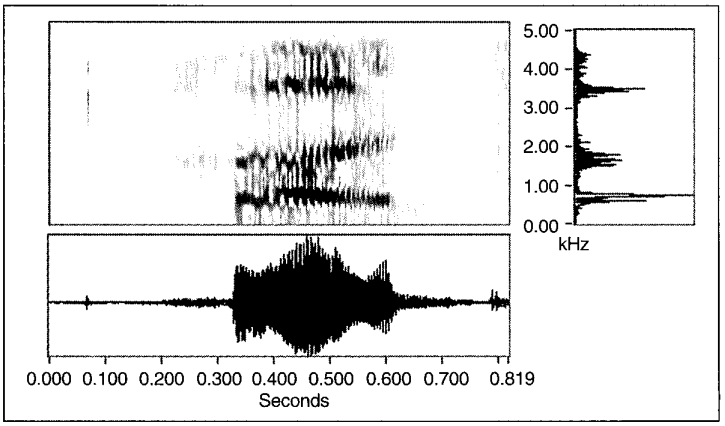

▲ 2. "Hood" (data courtesy of Y. Zhao, the Beckman Institute at the University of Illinois).

If a physician uses a ruler whose smallest scale is the decimeter to measure a patient's height, then there is no way to tell the patient's height in terms of centimeters.

which is known as an expansion or series.

When the set of $\{\psi_n\}_{n\in Z}$ forms a frame [21], a family of vectors that characterizes any signal from its inner products (or scalar product) as in (2) and (3), there will be a dual set $\{\hat{\psi}_n\}_{n\in Z}$ such that the expansion coefficients can be computed by

$$a_n=\langle s,\hat{\psi}_n\rangle=\int_{-\infty}^{\infty} s(t)\hat{\psi}_n^*(t)dt \tag{2}$$

for continuous-time signals, or

$$a_n=\langle s,\hat{\psi}_n\rangle=\sum_{k=-\infty}^{\infty} s[k]\hat{\psi}_n^*[k] \tag{3}$$

for discrete-time signals. "*" in (2) and (3) denote the complex conjugate operation. In electrical engineering, formulae (2) and (3) are known as transformations and $\hat{\psi}_n(t)$ is called the analysis function. Accordingly, (1) is known as an inverse transform and $\psi_n(t)$ is called the synthesis function.

The inner product has an explicit physical interpretation, which reflects the similarity between the signal $s(t)$ and the dual function $\hat{\psi}_n(t)$. In other words, the larger the inner product a_n, the closer the signal $s(t)$ is to the dual function $\hat{\psi}_n(t)$. $\{a_n\}$ depicts the signal's behavior in the $\hat{\Psi}$ domain.

The operation of the inner product in (2) and (3) may be thought of as using a ruler, constituted by a set of functions $\{\hat{\psi}_n\}$, to measure the signal under investigation. Each individual function can be considered as the tick mark of the ruler. The expansion coefficient $\{a_n\}$ indicates the weight of the signal's projection on the tick mark determined by $\hat{\psi}_n$. We all know that the precision of any measurement largely depends on the smallest unit used. If a physician uses a ruler whose smallest scale is the decimeter to measure a patient's height, then there is no way to tell the patients height in terms of centimeters. The goodness of the ruler is measured by the fineness of the unit. So, elementary functions for the signal expansion should be chosen such that the resulting tick mark is the finest.

For a given frame $\{\psi_n\}_{n\in Z}$, its corresponding dual frame is generally not unique. One particularly interesting scenario is $\hat{\psi}_n(t)=c\psi_n(t)$, where c denotes a constant number. In this case, we name $\{\psi_n\}_{n\in Z}$ as a tight frame. For the tight frame, the expansion coefficients $c\{a_n\}$ are exactly the signal's projection of the synthesis functions, up to a constant multiplier c. When the dual frame is not unique, the resulting expansion is redundant.

When the dual frame $\{\hat{\psi}_n\}_{n\in Z}$ is unique, then the set of $\{\psi_n\}_{n\in Z}$ forms a basis and there is no redundancy. In this case,

$$\langle\psi_n,\hat{\psi}_n\rangle=c\delta[n-n'] \tag{4}$$

where

$$\delta[n]=\begin{cases}1 & n=0\\ 0 & \text{otherwise}\end{cases}. \tag{5}$$

If $\hat{\psi}_n=c\psi_n$, then $\langle\psi_n,\hat{\psi}_n\rangle=c\delta[n-n']$ and $\{\psi_n\}_{n\in Z}$ are orthogonal. Otherwise, $\{\psi_n\}_{n\in Z}$ and $\{\hat{\psi}_n\}_{n\in Z}$ are biorthogonal, when $\{\psi_n\}_{n\in Z}$ forms a basis. For the biorthogonal expansion, the signal's feature described by the coefficients $\{a_n\}$ may not have obvious relations with the set of the basis function $\{\psi_n\}_{n\in Z}$ [Fig. 3(a)]. For the orthogonal expansion, however, the expansion coefficients $\{a_n\}$ must be the signal's projection on the basis function $\{\psi_n\}_{n\in Z}$ [Fig. 3(b)]. Moreover, in all cases, the positions of ψ_n and $\hat{\psi}_n$ are interchangeable. That is, either of them could be used for analysis or synthesis.

The concepts introduced above can also be understood from the matrix operation point of view. Suppose that the length of the signal $\vec{s}$ is L. We have the matrix G with dimension $M\times L$ and the matrix H with dimension $L\times M$, where $M\geq L$. If

$$H_{LM}G_{ML}\vec{s}=\vec{s} \tag{6}$$

for all vectors $\vec{s}$ with L elements, then we say that the space constituted by the matrix H is complete. Note, that in general, the matrix G could not be unique. If $M=L$ (H and G are square matrices), then G must be equal to H^{-1}. In this case, H and G are said to be biorthogonal to each other. If $G=H^{-1}=H^H$, H and G are orthogonal. The superscript "H" denotes the Hermitian conjugate. In both biorthogonal and orthogonal cases, the matrix G is unique.

Because $HG=I$ (6), taking the transpose, with respect to HG, yields,

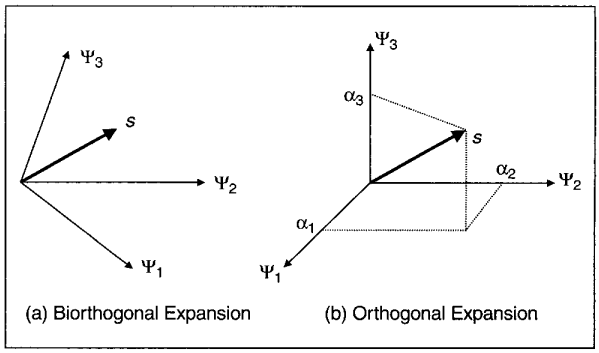

3. In both cases, $\{\psi_n\}_{n\in Z}$ is complete for three-dimensional space, but in orthogonal expansion, expansion coefficients a_n are exactly the signal's projection on the elementary functions ψ.

The elementary functions employed in the Fourier series extend from negative infinite time to positive infinite time, and are not associated with a particular instant in time.

$$H_{LM}G_{ML}s=(G_{ML})^{H}(H_{LM})^{H}\bar{s}=\bar{s} \tag{7}$$

which indicates that either H or G can be used as analysis (or synthesis). The two most fundamental questions for the expansion are

- How to build a meaningful set of functions $\{\psi_n\}_{n\in Z}$
- How to compute the corresponding set of dual functions $\{\hat{\psi}_n\}_{n\in Z}$.

One of the most well-known expansions is the Fourier series. For a periodic signal $\tilde{s}(t)$ with a period T, the Fourier series is defined as

$$\tilde{s}(t)=\sum_{n=-\infty}^{\infty}a_n e^{j2\pi nt/T}. \tag{8}$$

Because the elementary functions $e^{j2\pi nt/T}$ in (8), harmonically related complex sinusoidal functions, are orthonormal with respect to the scalar product, the dual function and the elementary function have the same form. Hence, we can readily obtain the expansion coefficients of the Fourier series in (8) by the regular inner product operation (2), e.g.,

$$a_n=\int_{-T/2}^{T/2}\tilde{s}(t)e^{-j2\pi nt/T}dt \tag{9}$$

which indicates the similarity between the signal and a set of harmonically related complex sinusoidal functions $\{e^{j2\pi nt/T}\}$. Because $e^{j2\pi nt/T}$ corresponds to impulses in the frequency domain, the ruler used for the Fourier transform possesses the finest frequency tick marks (that is, the finest frequency resolution). Consequently, the measurements, the Fourier coefficients $\{a_n\}$, precisely describe the signal's behavior at the frequency $2\pi n/T$.

For a non-periodic signal $s(t)$ in L^2, we have

$$s(t)=\frac{1}{2\pi}\int_{-\infty}^{\infty}S(\omega)e^{jt\omega}d\omega \tag{10}$$

and the Fourier transform

$$s(\omega)=\int_{-\infty}^{\infty}s(t)e^{-jt\omega}dt. \tag{11}$$

Conventionally, the square of Fourier transform is named the power spectrum. According to the Wiener-Khinchin theorem, the power spectrum can also be considered as the Fourier transform of the correlation function, i.e.,

$$P(\omega)=|S(\omega)|^2=\int_{-\infty}^{\infty}R(\tau)e^{-j\omega\tau}d\tau \tag{12}$$

where the correlation function $R(\tau)$ is the average of the instantaneous correlation $s(t)s(t-\tau)$, i.e.,

$$R(\tau)=\int_{-\infty}^{\infty}s(t)s^*(t-\tau)dt=\int_{-\infty}^{\infty}s(t+\tau/2)s^*(t-\tau/2)dt. \tag{13}$$

Note that the averaging process removes all time information from $R(\tau)$.

Finally, the reader should bear in mind that a function's time and frequency properties are not independent. They are linked by the Fourier transform. For example, we can't find a function that has an arbitrarily short time duration and narrow frequency bandwidth at the same time. If a function has a short time duration, its frequency bandwidth must be wide, or vice versa. From the uncertainty principle point of view, it is the Gaussian-type signal, such as

$$g(t)=\left(\frac{\alpha}{\pi}\right)^{\frac{1}{4}}\exp\{-\alpha t^2\} \tag{14}$$

that achieves the optimal joint time-frequency concentration. The balance of the time and the frequency concentration is controlled by the parameter α. The smaller the value of α, the narrower the frequency bandwidth (longer time duration), or vice versa.

Gabor Expansion

As mentioned in the preceding section, the classical Fourier series is unsuitable for characterizing signals that only last for a short time or whose frequency contents change over time. The reason for this is that the elementary functions employed in the Fourier series extend from negative infinite time to positive infinite time, and are not associated with a particular instant in time. In other words, the tick mark adopted by the classical Fourier transform does not contain time information.

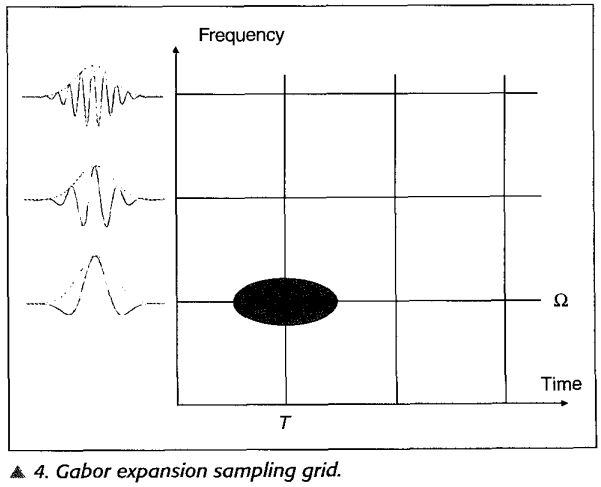

▲ 4. Gabor expansion sampling grid.

Gabor Expansion and Short-Time Fourier Transform

In 1946, Dennis Gabor, a Hungarian-born British physicist, suggested expanding a signal into a set of functions that are concentrated in both the time and frequency domains [26]. (In 1970, Gabor was awarded the Nobel Physics Prize for his discovery of the principles underlying the science of holography.) Then, use the coefficients as the description of the signal's local property. The resulting representation is now known as the *Gabor expansion*,

$$s(t)=\sum_{m=-\infty}^{\infty}\sum_{n=-\infty}^{\infty}C_{m,n}h_{m,n}(t) \tag{15}$$

where $C_{m,n}$ are called the Gabor coefficients. The set of elementary functions $\{h_{m,n}(t)\}$ consists of a time- and frequency-shifted function $h(t)$, i.e.,

$$h_{m,n}(t)=h(t-mT)e^{jn\Omega t}. \tag{16}$$

In Gabor's original paper, $h(t)$ is the normalized Gaussian function $g(t)$, defined in (14), because it is optimally concentrated in the joint time-frequency domain, in terms of the uncertainty principle. The parameters T and Ω are time and frequency sampling steps, respectively. The product of $T\Omega$ determines the density of the sampling grid. The smaller the product, the denser the sampling.

Fig. 4 illustrates the elementary functions used in the Gabor expansion and the Gabor expansion-sampling grid. Because the frequency-shifted Gaussian functions have a short time duration, the Gabor expansion is more suitable for characterizing transients and signals with sharp changes (Fig. 1). The time and the frequency resolutions of $h_{m,n}(t)$ can be adjusted by the parameter α in (14). The smaller the value of α, the better the frequency resolution (poorer time resolution), or vice versa. Because $h_{m,n}(t)$ are concentrated in $[mT, n\Omega]$, Gabor suggested that the coefficient $C_{m,n}$ reflected a signal's behavior in the vicinity of $[mT, n\Omega]$. As a matter of fact, that is not really true, because $\{h_{m,n}(t)\}$ in general does not form a tight frame. Consequently, the Gabor coefficients $C_{m,n}$ are not a signal's projection on $h_{m,n}(t)$. We shall elaborate on this issue later.

Gabor had the clear insight to see the potential of this expansion, and it was to a great extent, his work and his claims that spurred much of the subsequent work on joint time-frequency analysis. However, he did not actually contribute to the mathematical theory of the Gabor expansion. Many important aspects of the Gabor expansion were not known during his lifetime [24], [29]-[31].

Moreover, Gabor limited $h(t)$ to be the Gaussian function and $T\Omega = 2\pi$. In fact, as long as the sampling grid is dense enough, for instance,

$$T\Omega \le 2\pi \tag{17}$$

all those commonly used analysis functions, such as the exponential, rectangular, and Gaussian-type functions,

Gabor had the clear insight to see the potential of this expansion, and it was to a great extent, his work and his claims that spurred much of the subsequent work on joint time-frequency analysis.

can be used in the Gabor expansion. When the product $T\Omega = 2\pi$, it is considered critical sampling. When $T\Omega < 2\pi$, it is oversampling. Note that the set of $\{h_{m,n}(t)\}$ in general won't be orthogonal unless $h_{m,n}(t)$ are poorly concentrated in either the time or the frequency domain. If $\{h_{m,n}(t)\}$ are not orthogonal, then the estimation of the Gabor coefficients $C_{m,n}$ won't be trivial. A natural question at this point is "How do we compute the Gabor coefficients?" If the Gabor coefficients are not unique, which one can better describe a signal's time and frequency behavior jointly? Before we answer these questions, let's review another approach, the short-time Fourier transform (STFT), which appeared at about the same time as the introduction of the Gabor expansion [32].

While Gabor focused on the expansion, the STFT modified the Fourier transform (inner products of $s(t)$ and $e^{j\omega t}$). Instead of processing the entire signal at once, STFT takes the Fourier transform (FT) on a block by block basis (Fig. 5). Therefore, the resulting Fourier transform can then be thought of as a signal's frequency behavior during the time period covered by the data block. The procedure can be described by

$$STFT[mT,n\Omega]=\int_{-\infty}^{\infty}s(t)\gamma^*(t-mT)e^{-jn\Omega t}dt \tag{18}$$

where the analysis window function $\gamma(t)$ balances the time and frequency resolutions. The smaller the time duration of $\gamma(t)$, the better the time resolution (poorer frequency resolution). The blocks could be overlapped or disjointed. The percentage of overlap between each block

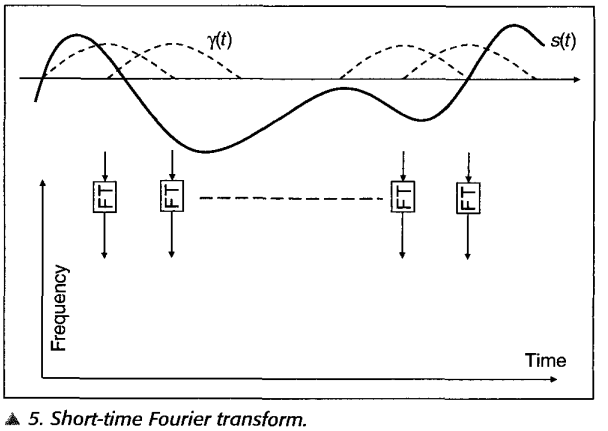

▲ 5. Short-time Fourier transform.

is determined by the time sampling step T and the length of the analysis window function $\gamma(t)$.

Let us rewrite (18) in the regular inner product form, i.e.,

$$STFT[mT,n\Omega]=\int_{-\infty}^{\infty} s(t)\gamma^*_{m,n}(t)dt \tag{19}$$

where

$$\gamma_{m,n}(t)=\gamma(t-mT)e^{jn\Omega t}. \tag{20}$$

Note that (20) and (16) have exactly the same form; both are time- and frequency- shifted versions of a single prototype function. Let $C_{m,n}$ = STFT[mT, $n\Omega$], then (15) and (19) form a pair of Gabor expansions. The relationship between $\gamma(t)$ and $h(t)$ is

$$\sum_{m=-\infty}^{\infty}\sum_{n=-\infty}^{\infty} h_{m,n}(t)\gamma^*_{m,n}(\tau)=\delta(t-\tau) \tag{21}$$

which is known as a formal identity. Equations (19) and (15) indicate that the STFT is, in fact, the Gabor coefficient. Conversely, the Gabor expansion can be thought of as the inverse of the STFT. However, these relationships were not widely understood until the early '80s [3]-[5].

Traditionally, we investigate signals and systems in the time or the frequency domain separately. The Gabor expansion pair, (19) and (15), now allow us to map time-domain functions into the joint time-frequency domain. This has been found extremely helpful when the system to be analyzed is time variant.

Importantly, for a given time function $s(t)$ and analysis window function $\gamma(t)$, we are always able to find the joint time-frequency function $C_{m,n}$. However, for an arbitrary 2D function, there may be no corresponding signal $s(t)$ and window function $\gamma(t)$. The set of $\{C_{m,n}\}$ is a subspace of the entire set of 2D functions (Fig. 6).

The key issue of the Gabor expansion is how to compute the dual function $\gamma(t)$ for a given $h(t)$. Except for a few functions at critical sampling [4], [22], [25], the analytical solutions of (21), in general, do not exist. This fact inspired many researchers to seek the discrete version of the Gabor expansion. Recently, one of the major advances in the study of the Gabor expansion is the discovery of the discrete version [33], [34], [37], [44], [63], [72]. Although there were some discrete versions of the inverse STFT [40] suggested before, they were not motivated by expansion and inner product operations. Some important aspects, such as the relationship between oversampling and perfect reconstruction were not clear. In particular, the summation of computing the dual function derived previously, was generally unbounded, which is not directly suitable for numerical implementation. By using digital computers, we can now readily compute the Gabor expansion and apply it to real-world problems.

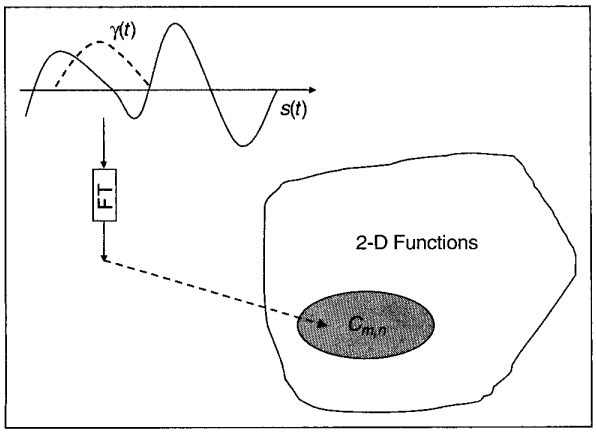

▲ 6. The Gabor coefficients are a subset of the set of 2D functions. An arbitrary 2D time-frequency function may not be a valid $C_{m,n}$.

Discrete Gabor Expansion

Applying the sampling theorem and the Poisson-sum formula [44], [63], we derive the discrete Gabor expansion as

$$s[i]=\sum_{m}\sum_{n-0}^{N-1} C_{m,n}h[i-m\Delta M]W_N^{ni} \tag{22}$$

where

$$W_N^{ni}=\exp\left\{j\frac{2\pi ni}{N}\right\}$$

and

$$C_{m,n}=\sum_{i} s[i]\gamma^*[i-m\Delta M]W_N^{-ni} \tag{23}$$

where ΔM denotes the discrete time sampling interval. N indicates the number of frequency channels. The ratio $N/\Delta M$ is considered as the oversampling rate. For a stable reconstruction, the oversampling rate must be more than or equal to one. Usually, we require that L is evenly divisible by N and ΔM. The number of frequency bins N is a power of two.

The dual function can be solved by ΔM independent linear systems [47], i.e.,

$$A_k\bar{\gamma}^*_k=\bar{\mu}_k \qquad k=0,1,2,...\Delta M-1 \tag{24}$$

where the elements of the matrix A_k and vectors $\bar{\gamma}_k$ and $\bar{\mu}_k$ are defined as

$$a_k(q,p)\equiv\tilde{a}[k+p\Delta M+qN]$$
$$\gamma_k(p)\equiv\gamma[k+p\Delta M]$$
$$\mu_k(q)\equiv(N^{-1},0,0,...)^T$$

where $0\le p<L/\Delta M$, and L denotes the length of $h[i]$ and $\gamma[i]$. The periodic auxiliary function $\tilde{a}[i]$ is given by

$$\tilde{a}[i+nL]=\begin{cases}h[i] & 0\le i<L\\ 0 & L\le i<2L-N\end{cases} \qquad 0\le q<\frac{2L}{N}-1. \tag{25}$$

When the signal length is equal to the length of $h[i]$ and $\gamma[i]$ [63], we can also simply let

$$\tilde{a}[i+nL]=h[i] \qquad 0\le q<\frac{L}{N}. \tag{26}$$

In this case, the solution of $\gamma[i]$ almost always exists! But, the samples have to be periodically extended. Hence, it is only suitable for finite and small number of samples. On the other hand, using (25), we can impose any type of extension on the samples, which enables us to perform on-line processing. Moreover, this method guarantees that the length of the dual window will always be the same as the length of the original window.

Orthogonal-Like Gabor Expansion

When $N = \Delta M$ (critical sampling), the solution of $\gamma[i]$ in (24) is unique (thereby the Gabor coefficients $C_{m,n}$ are unique). Fig. 7 illustrates the dual function $\gamma[i]$ of the normalized Gaussian function $g[i]$ in (14) at critical sampling. Note that in this case, $\gamma[i]$ is concentrated neither in time nor in frequency.

According to (23), the Gabor coefficients $C_{m,n}$ are inner products of $s[i]$ and $\gamma_{m,n}[i]$, which reflect the similarity between $s[i]$ and $\gamma_{m,n}[i]$. If $\gamma[i]$ is badly localized, then the Gabor coefficients $C_{m,n}$ will fail to describe the signal's property in the vicinity of $[m\Delta M, n]$, no matter how $h[i]$ is concentrated. To ensure that the Gabor coefficients $C_{m,n}$ indeed characterize a signal's properties around $[m\Delta M, n]$, we have to make $\gamma[i]$ concentrated in both the time and frequency domains. Once the function $h[i]$ is selected to be optimally concentrated (as it always is), the natural solutions of $\gamma[i]$ are those which are similar to the predetermined $h[i]$, i.e.,

$$\min_{\text{dual relation}} \left\| \frac{\bar{\gamma}}{|\bar{\gamma}|} - \bar{h} \right\|^2 \tag{27}$$

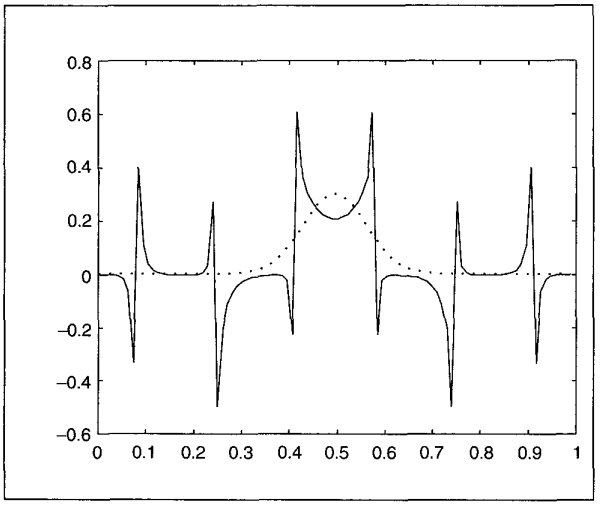

▲ 7. Dual function $\gamma(t)$ (solid line) for the normalized Gaussian function $g(t)$ (dotted line) at critical sampling.

In many applications, such as subband echo cancellation, the Gabor-expansion-based filter banks have been found to be superior to wavelet-based filter banks.

where $h[i]$ is assumed to be normalized. The dual relation is described by (24). It is interesting to know that the optimal solution of (27) is the minimum norm of (24)!

When $h[i]$ is a discrete version of the normalized Gaussian function in (14), the error in (27) is a function of variance α and a sampling pattern determined by ΔM and N. It is observed that the minimum error occurs when $\alpha = \pi/(N\Delta M)$ [44]. Fig. 8 demonstrates $h[i]$ and corresponding $\gamma_{\text{opt}}[i]$. Note that the difference between $h[i]$ and $\gamma_{\text{opt}}[i]$ is inversely proportional to the oversampling rate. For critical sampling, the solution of $\gamma[i]$ is unique. As the oversampling rate increases, $a = N/\Delta M$, $\gamma_{\text{opt}}[i]$ becomes closer to $h[i]$.

If $\gamma[i]$ is closer to $h[i]$, for instance, $\gamma[i] \approx c\,h[i]$, then we can rewrite (22) and (23) as

$$s[i]=\sum_m \sum_{n=0}^{N-1} C_{m,n} h[i-m\Delta M] W_N^{ni}$$

$$C_{m,n} \approx c \sum_i s[i] h^*[i-m\Delta M] W_N^{-ni}.$$

Although the set of $\{h_{m,n}[i]\}$ may not be linearly independent, the Gabor coefficients $C_{m,n}$ are indeed the orthogonal projection on $\{h_{m,n}[i]\}$. So, we name it as an orthogonal-like Gabor expansion. For the orthogonal-like Gabor expansion, the Gabor coefficients $C_{m,n}$ will well characterize the signal's behavior in the vicinity of $[m\Delta M, n]$ as long as $h_{m,n}[i]$ is concentrated in $[m\Delta M, n]$.

The optimization in (27) can also be considered a process to pursue the near tight frame. Finally, the discrete Gabor expansion, (22) and (23), can be thought of as a set of perfect reconstruction filter banks [54], [58]. Because (22) and (23) can be realized by the FFT and inverse FFT, the implementation of the Gabor-expansion-based filter banks is very efficient. In many applications, such as subband echo cancellation, the Gabor-expansion-based filter banks have been found to be superior to wavelet-based filter banks [35].

Time-Varying Filtering

One of the most important applications of joint time-frequency representations such as the Gabor expansion, is the detection and estimation of noise-corrupted signals [70]. While random noise tends to spread evenly into the entire joint time-frequency domain, the signal energy is usually concentrated in a relatively small region. Consequently, the regional signal-to-noise ratio (SNR)

can be substantially improved in the joint time-frequency domain [71].

Fig. 9 depicts the impulse signal received by the U.S. Department of Energy ALEXIS/BLACKBREAD satellite. After passing through dispersive media, such as the ionosphere, the impulse signal becomes a nonlinear chirp signal. While the time waveform is severely corrupted by random noise, the power spectrum is dominated mainly by radio carrier signals that are basically unchanged over time (Fig. 9, again). In this case, neither the time waveform nor the power spectrum indicate the existence of the impulse signal. However, when looking at the plot of $|C_{m,n}|$, we can immediately identify the presence of the chirp-type signal arching across the joint time-frequency domain. This observation suggests that we can use a mask to filter out the desired Gabor coefficients $\{C_{m,n}\}$ from the noise background and then reconstruct the time waveform via the Gabor expansion.

The problem here is that the Gabor coefficients are a subset of the set of 2D functions. Usually, the modified $\{C_{m,n}\}$ are no longer in the set of valid Gabor coefficients. In this case, for a given modified $\{C_{m,n}\}$, there may not be an existing signal that corresponds to it. For the sake of presentation simplicity, let us write (22) in matrix form, i.e.,

$$\vec{s} = H\vec{c} \tag{28}$$

where $\vec{s}$, H, and $\vec{c}$ denote the signal vector, synthesis matrix, and Gabor coefficients vector. The matrix form of (23) is

$$\vec{c} = G\vec{s} \tag{29}$$

where G denotes the analysis matrix. If H and G satisfy the dual relation determined by (24), then $HG = I$ and

$$\vec{s} = H\vec{c} = HG\vec{s}. \tag{30}$$

Note that H and G, in general, are not square matrices except for critical sampling. Let $\vec{c}_d$ denote the modified and desired Gabor coefficients, that is,

$$\vec{c}_d = \Phi\vec{c} = \Phi G\vec{s} \tag{31}$$

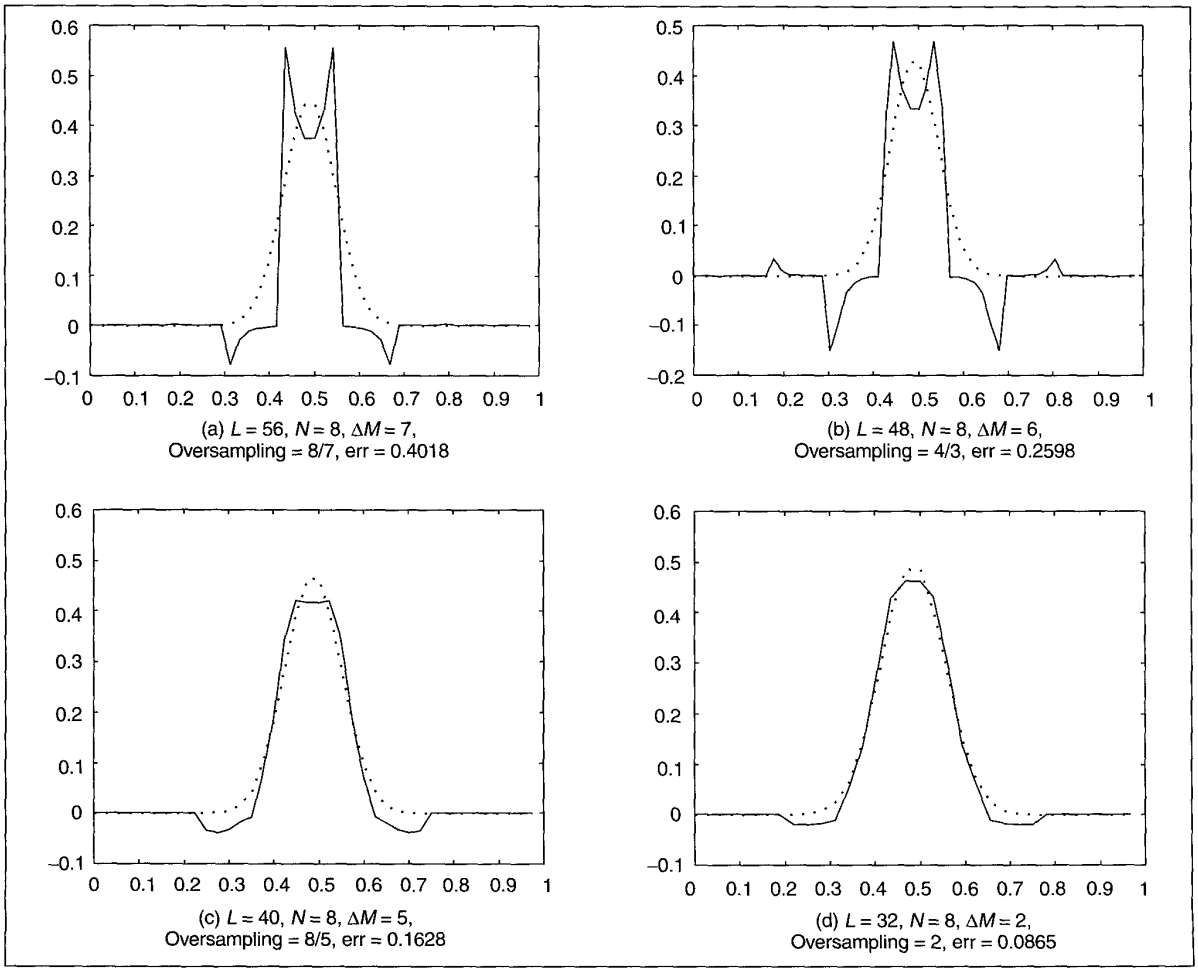

8. h[i] (dotted line) and $\gamma_{opt}[i]$ (solid line) (as the oversampling rate increases, $\gamma_{opt}[i]$ becomes more and more close to h[i]).

where Φ is a diagonal matrix whose diagonal elements are either one or zero. Based on $\vec{c}_d$ we compute a time waveform $\vec{s}_1$,

$$\vec{s}_1 = H\vec{c}_d .$$

Because the modified Gabor coefficients are generally not valid Gabor coefficients,

$$G\vec{s}_1 \neq \vec{c}_d \tag{31}$$

which says that the joint time-frequency properties of $\vec{s}_1$ are not the same as the desired Gabor coefficients $\vec{c}_d$.

A common approach is to seek a $\vec{s}_{\text{opt}}$ such that the distance between the Gabor coefficients of $\vec{s}_{\text{opt}}$ and the desired Gabor coefficients $\vec{c}_d$ is minimum, that is,

$$\min \left\| \vec{c}_d - G\vec{s}_{\text{opt}} \right\| \tag{32}$$

which is known as the least square error (LSE) method. It is well known that the solution of (32) is the pseudoinverse of G, that is,

$$\vec{s}_{\text{opt}} = (G^T G)^{-1} G^T \vec{c}_d . \tag{33}$$

Fig. 10 illustrates the LSE algorithm.

The LSE has been widely used and extensively studied for many years [7], [23], [27], [65]. But it may not be the best solution for many applications. In particular, to solve the LSE, we need to compute the pseudoinverse, which is computationally intensive and memory demanding. When the data includes over 10,000 samples, it would be difficult to apply an LSE algorithm with conventional PCs. A more efficient method developed recently is an iterative algorithm in which we continuously apply the same mask and reconstruct the time waveform. The procedure can be summarized as follows:

$$\vec{s}_1 = H\vec{c}_d$$
$$\vec{c}_1 = \Phi G\vec{s}_1 = \Phi GH\vec{c}_d$$
$$\vec{s}_2 = H\vec{c}_1$$
$$\vec{c}_2 = \Phi G\vec{s}_2 = \Phi GH\vec{c}_1 = (\Phi GH)^2 \vec{c}_d$$
$$\vec{c}_k = \Phi G\vec{s}_k = (\Phi GH)^k \vec{c}_d .$$

The sufficient condition for the iteration above to converge can be found in [69]. Under that condition,

- $\vec{c}_k$ converges to inside of Φ;
- The result of the first iteration $\vec{s}_1$ is equivalent to $\vec{s}_{\text{opt}}$ computed by the LSE method.

Two trivial cases, $h[i] = \gamma[i]$ or critical sampling ($\{h_{m,n}\}$ forms a basis), satisfy the sufficient condition [69]. For critical sampling, the modified Gabor coefficients are always valid Gabor coefficients, that is,

$$G\vec{s}_1 = \vec{c}_d . \tag{34}$$

In this case, the iteration converges at the first step. However, critical sampling often leads to bad localization of the dual function $\gamma[i]$, and, as pointed out earlier, it is less interesting in applications. On the other hand, $h[i] = \gamma[i]$ usually implies high oversampling and thereby heavier computation. To reduce the computational burden in real applications, we employ the orthogonal-like Gabor expansion introduced in the preceding section. Although $\gamma[i]$ is hardly exactly equal to $h[i]$, the performance of the orthogonal-like, Gabor-expansion-based algorithm has been found to be good enough for most applications.

Fig. 11 plots the simulation results for the example illustrated in Fig. 9. Fig. 11(a) depicts the error vs. the number of iterations, which shows the iteration exponentially converging. Note that there is a substantial improvement between the first and second iterations. The result obtained by the first iteration is closer to that computed by the LSE method. But, they are generally not equal unless the convergence condition [69] is truly met. In many applications, the LSE solution often is not the best one. Fig. 11(b) depicts the reconstructed signal after 30 iterations. In this example, the number of samples is 9000, which is impossible to be solved by the LSE de-

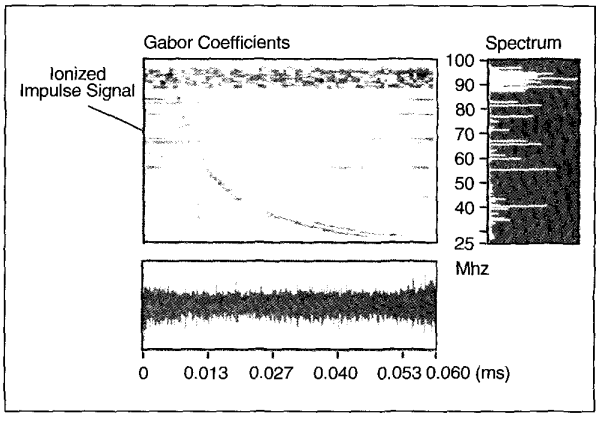

9. Due to the low SNR, the ionized impulse signal cannot be recognized in either time or frequency domains. However, from $|C_{m,n}|$ we can readily distinguish it. (Data courtesy of the Nonproliferation and international security division, Los Alamos National Laboratory.)

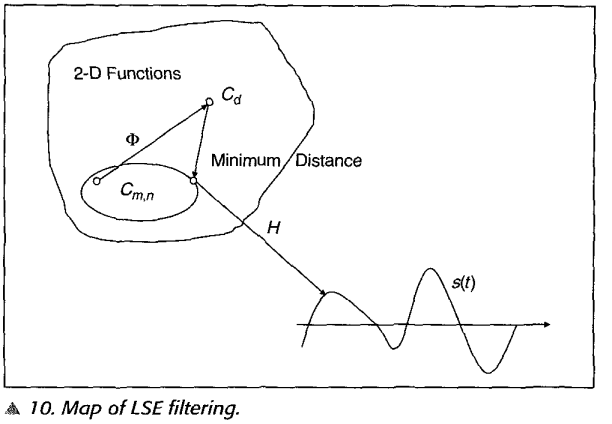

10. Map of LSE filtering.

scribed by (33) due to the computational complexity and memory limitations. The iterative algorithm not only yields a better SNR, but also is practical for online implementation.

Time-Dependent Spectrum

Besides the linear transforms, such as the Gabor expansion and wavelets, another important method for the joint time-frequency analysis is the time-dependent spectrum. The goal here is to seek a representation that describes a signal's power spectrum changing over time. Analogous to the conventional power spectrum, a straightforward approach of computing the time-dependent spectrum is to take the square of the STFT, the counterpart of the classical Fourier transform, i.e.,

$$P(t,\omega)=\left|\int_{-\infty}^{\infty} s(\tau)\gamma(\tau-t)e^{-j\omega\tau}d\tau\right|^2. \tag{35}$$

We call it the STFT-based spectrogram to distinguish it from the Gabor-expansion-based spectrogram introduced later.

Fig. 12 illustrates the STFT-based spectrogram for a linear chirp signal. While the time waveform (bottom plot) and classical power spectrum only tell a part of the signal's behavior, the STFT-based spectrogram indicates how the linear chirp signal's frequencies change over time. The main problem of the STFT-based spectrogram is that it suffers from the so-called window effect. As shown in Fig. 12, the width of $\gamma(t)$ governs the resulting time and frequency resolutions. In the left plot, a short time duration window function is used, whereas the right plot uses a long time duration window. Obviously, the left plot has better time resolution (poor frequency resolution). On the other hand, the right one has poor time resolution (better frequency resolution). Although the STFT-based spectrogram is simple and easily implemented, it has been found inadequate for the applications where both high time and frequency resolutions are required.

Wigner-Ville Distribution

As mentioned in the preceding section (12), the conventional correlation, in fact, is the average of instantaneous correlations $s(t+\tau/2)s^*(t-\tau/2)$, i.e.,

$$R(\tau)=\int_{-\infty}^{\infty} s(t+\tau/2)s^*(t+\tau/2)dt=\int_{-\infty}^{\infty} R(t,\tau)dt. \tag{36}$$

By averaging the instantaneous correlations, we lose the time information. How about using $R(t,\tau)$ to replace $R(\tau)$? For instance,

$$WVD(t,\omega)=\int_{-\infty}^{\infty} R(t,\tau)e^{-j\omega\tau}dt. \tag{37}$$

Obviously, there is no window effect. Compared to the STFT-based spectrogram, as we shall see later, (37) can better characterize a signal's properties in the joint time-frequency domain. Formula (37) is known as the Wigner-Ville distribution (WVD), which was originally developed in the area of quantum mechanics by a Hun-

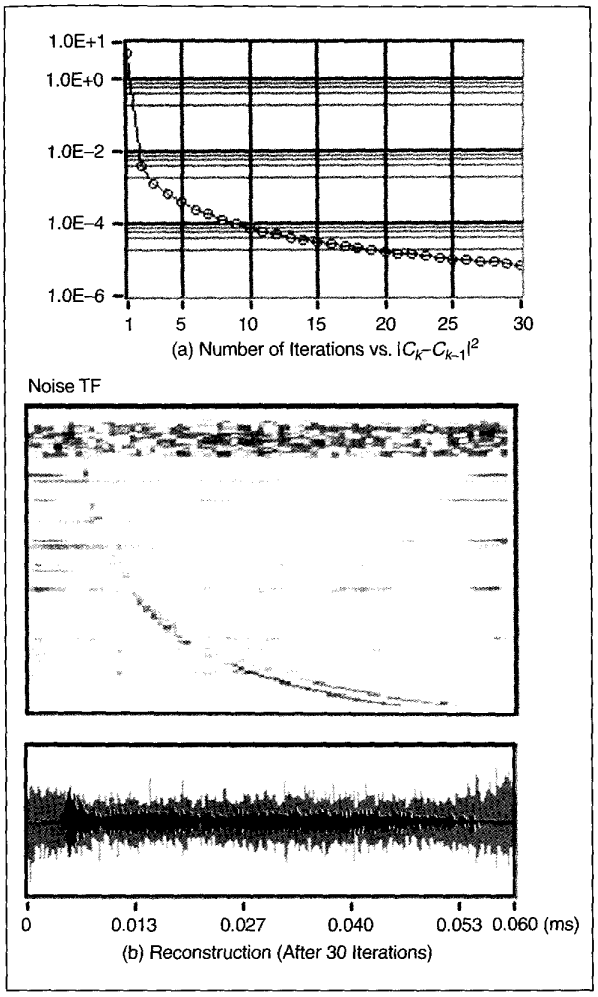

▲ *11. Error (a) and reconstruction (b).*

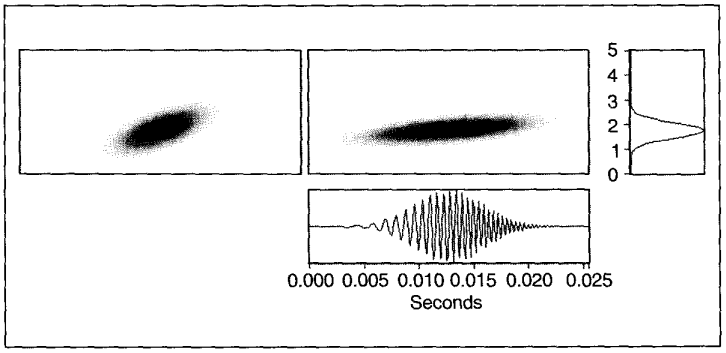

▲ *12. The STFT-based spectrogram for a linear chirp signal (The results are subject to the selection of the analysis window function. The short time duration window (left) leads to good time resolution and poor frequency resolution, or vice versa).*

It is the crossterm interference that prevents the Wigner-Ville distribution from being used for real applications, though it possesses many desirable properties for signal analysis.

garian-born American physicist, Eugene P. Wigner [64], in 1932. Fifteen years later, it was introduced into the signal processing area by a French scientist J. Ville [59]. (Wigner's pioneering application of group theory to an atomic nucleus established a method for discovering and applying the principles of symmetry to the behavior of physical phenomena. In 1963, he was awarded the Nobel Physics Prize.)

Let $s(t)=A(t)e^{j\phi(t)}$, where both $A(t)$ and $\phi(t)$ are real-valued time functions. Then, the first derivative of the phase $\phi(t)$ represents the weighted average of the instantaneous frequency. Traditionally, the first derivative of the phase is called the instantaneous frequency, which is actually incorrect for several reasons. For example, $\phi'(t)$ is a single-valued function, whereas at each time instant, generally there are multiple frequencies.

We can prove that the mean frequency of the WVD at time t is truly equal to the signal's weighted average instantaneous frequency, i.e.,

$$\frac{\int_{-\infty}^{\infty}\omega WVD(t,\omega)d\omega}{\int_{-\infty}^{\infty}WVD(t,\omega)d\omega}=\phi'(t)\,. \tag{38}$$

Therefore, the WVD indeed describes the signal's joint time-frequency behavior. Moreover, the energy of the WVD is the same as the energy content in the signal $s(t)$, i.e.,

$$\frac{1}{2\pi}\int_{-\infty}^{\infty}\int_{-\infty}^{\infty}WVD(t,\omega)dtd\omega=\int_{-\infty}^{\infty}|s(t)|^2\,dt=\frac{1}{2\pi}\int_{-\infty}^{\infty}|S(\omega)|^2\,d\omega \tag{39}$$

As a result of this property, the WVD is often thought of as a signal's energy distribution in the joint time-frequency domain. It is interesting to note that all useful properties of the WVD [i.e., (38) and (39)] are associated with certain types of averages. The STFT-based spectrogram possesses neither (38) nor (39). Fig. 13 illustrates the WVD of the linear chirp signal. Compared to the STFT-based spectrogram in Fig. 12, the WVD has much better time and frequency resolutions.

The problem of the WVD is the so-called crossterm interference. As an example, let's look at two time- and frequency-shifted Gaussian functions in Fig. 14. From the time waveform and the power spectrum, we can easily distinguish those two components. Essentially, there is nothing in the vicinity of 2 kHz during the time interval from 0.01 ~ 0.015 s. However, the WVD plot shows a strongly oscillated term in that area. Because this term reflects the correlation of two signal components [47], it is named the crossterm. Although the average of the crossterm in this example is near to zero (in other words, it does not contribute energy to the signal), the magnitude of the crossterm can be proven to be twice as large as that of the signal terms. It is the crossterm interference that prevents the Wigner-Ville distribution from being used for real applications, though it possesses many desirable properties for signal analysis.

In what follows, we shall introduce two alternative methods, the Cohen's class and the Gabor spectrogram, to reduce the crossterm interference with limited affects on the useful properties. While the Cohen's class can be thought of as 2D linear filtering of the Wigner-Ville distribution, the Gabor spectrogram is a truncated Wigner-Ville distribution.

Cohen's Class

As mentioned previously, the crossterm is almost always strongly oscillated. So, an intuitive approach of removing

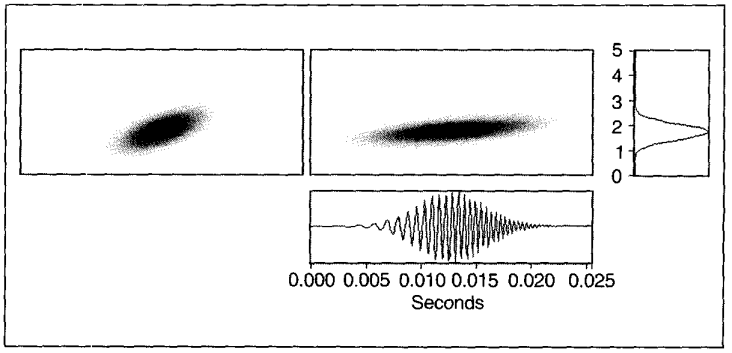

▲ *12. The STFT-based spectrogram for a linear chirp signal (The results are subject to the selection of the analysis window function. The short time duration window (left) leads to good time resolution and poor frequency resolution, or vice versa).*

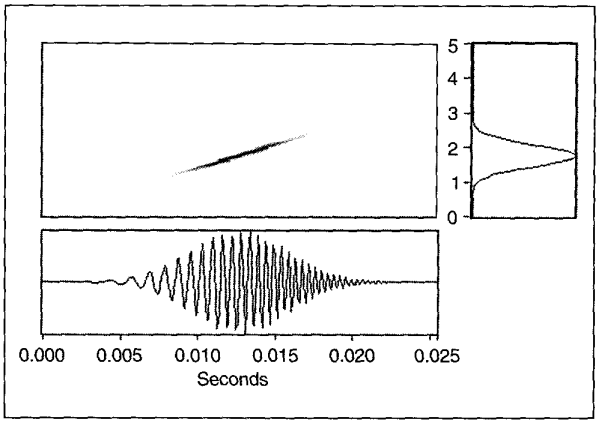

▲ *13. The WVD of a linear chirp signal.*

the crossterm is to apply a 2D low-pass filter $\phi(\omega,t)$ to the Wigner-Ville distribution, i.e.,

$$\frac{1}{2\pi}\int_{-\infty}^{\infty}\int_{-\infty}^{\infty}\phi(\mu,\tau)WVD(t-\mu,\omega-\tau)d\tau d\mu. \tag{40}$$

Expanding the term of WVD in the above equation yields

$$C(t,\omega)=\int_{-\infty}^{\infty}e^{-j\omega\tau}\int_{-\infty}^{\infty}\Phi(t-\mu,\tau)s(\mu+\frac{\tau}{2})s^*(\mu-\frac{\tau}{2})d\mu d\tau \tag{41}$$

where the function $\Phi(t, \tau)$ denotes the Fourier transform of $\phi(\mu, \tau)$. Formula (41) was first developed in the field of the quantum mechanics by Leon Cohen [17] and, it is named as Cohen's class. Because the kernel function $\Phi(t, \tau)$ [or $\phi(t, \omega)$] determines the property of (41), Cohen's class greatly facilitates the selection of our desired transformation. It is interesting to note that almost all previously known time-dependent spectra [38], [49] can be written in the form (41). The prominent members of Cohen's class include the STFT-based spectrogram, the Choi-Williams distribution [14], the cone-shaped distribution [74], the adaptive kernel representation [6], and the radial Butterworth kernel representation [67] and [68]. Comprehensive discussions of Cohen's class can be found in [16], [18], [19], [28], [47], and [66].

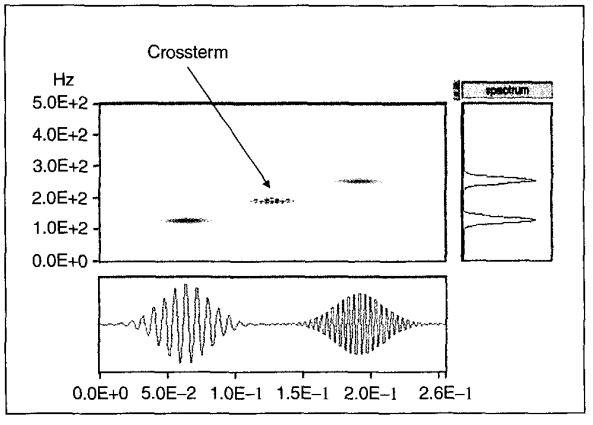

▲ *14. WVD of the sum of two Gaussian functions.*

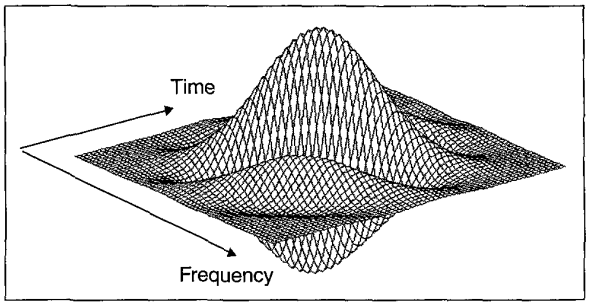

▲ *15. The signal energy in the joint time-frequency domain can be represented in terms of an infinite number of elementary energy atoms. All those atoms are concentrated, symmetrical, and oscillated. The amount of energy contained in each individual atom is inversely proportional to the rate of oscillation.*

Gabor Spectrogram

Another way of separating a signal's components in time and frequency is to apply the Gabor expansion [42], [46] as introduced in the preceding section. For example, we first expand the signal into,

$$s(t)=\sum_{m=-\infty}^{\infty}\sum_{n=-\infty}^{\infty}C_{m,n}h_{m,n}(t).$$

Then take the Wigner-Ville distribution on both sides to obtain

$$WVD(t,\omega)=\sum_{m=-\infty}^{\infty}\sum_{n=-\infty}^{\infty}\sum_{m'=-\infty}^{\infty}\sum_{n'=-\infty}^{\infty}C_{m,n}C^*_{m',n'}WVD_{h,h'}(t,\omega) \tag{42}$$

where $WVD_{h,h'}(t,\omega)$ denotes the WVD of two time- and frequency-shifted Gaussian functions defined in (16). As illustrated in Fig. 15, $WVD_{h,h'}(t,\omega)$ is concentrated, symmetrical, and oscillated. It can be shown that the energy of $WVD_{h,h'}(t,\omega)$ is inversely proportional to the rate of oscillation. If we consider $WVD_{h,h'}(t,\omega)$ as an energy atom, then (42) indicates that a signal's energy can be thought of as the sum of an infinite number of energy atoms. The contribution of each individual energy atom to the signal's energy not only depends on its weight, $C_{m,n}C^*_{m',n'}$, but also on the oscillation rate. The highly oscillated atoms are directly associated with crossterm interference, but have negligible influence to the signal energy [46], [47].

Based on the closeness of $h_{m,n}(t)$ and $h_{m',n'}(t)$ in the time and frequency domains, we rewrite (42) as

$$GS_D(t,\omega)=\sum_{|m-m'|+|n-n'|\le D}C_{m,n}C^*_{m',n'}WVD_{h,h'}(t,\omega) \tag{43}$$

which is known as the Gabor spectrogram (GS), because it is a Gabor expansion-based-spectrogram. The parameter D in (43) denotes the order of the GS. When $D = 0$, the GS only contains those terms in which $m = m'$ and $n = n'$. In other words, in this case, we only consider the correlation of two identical components. As the order D increases, increasingly more less-correlated components are included. When D goes to infinity, the GS converges to the WVD.

Fig. 16 depicts the WVD of an echo-location pulse emitted by the large brown bat, *Eptesicus fuscus*. In addition to the true signals, the WVD also exhibits strong crossterm interference. Fig. 17 illustrates the STFT-based spectrogram and Gabor spectrogram for the same bat sound. Obviously, as the order increases, the resolution improves. The best selection usually is $D = 3 \sim 4$. When D gets larger, the GS converges to the WVD. While the instantaneous frequencies computed by the STFT-based spectrogram are subject to the selection of the analysis window function, they are much closer to the real value in the Gabor spectrogram cases.

It is worth noting that the energy atom, $WVD_{h,h'}(t,\omega)$ in (43), has a closed form that can be saved as a table.

Consequently, once we obtain the Gabor coefficients $C_{m,n}$ (which can be efficiently computed by the windowed FFT), the rest of the process is nothing more than repeatedly using the look-up table.

In principle, we can also decompose other transforms, such as the Choi-Williams distribution, via a signal's Gabor expansion. It has been found, however, that the Wigner-Ville-distribution-based decomposition (42) has the best performance—a result of the energy atom $WVD_{b,b'}(t,\omega)$ in (42) being optimally concentrated in the joint time-frequency domain. Moreover, as previously mentioned, the energy atom $WVD_{b,b'}(t,\omega)$ has a closed form. Consequently, we don't need to compute it online, resulting in a tremendously improved computation speed.

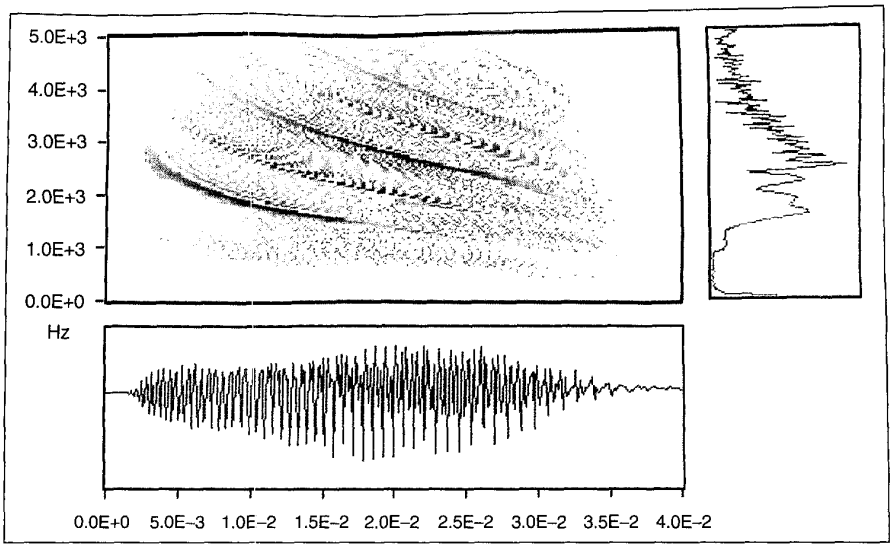

▲ *16. WVD of echo-location pulse (Bat data provided by Curtis Condon, Ken White, and Al Feng of the Beckman Institute at the University of Illinois).*

Parametric Time-Frequency Analysis

The joint time-frequency analysis methods presented so far are essentially nonparametric in that no model is assumed to be a priori. When the analyzed signal is discrete, the time and frequency resolutions of all those methods are subject to the number of data samples. In contrast with the nonparametric methods, there are several parametric approaches, such as the matching pursuit and adaptive spectrogram that have been proposed recently [36], [41], [43], [45]. In what follows, we shall briefly introduce the signal adaptive approximation and adaptive spectrogram.

Assume that the given data are samples of the signal $s(t)$, i.e.,

$$s(t)=\sum_{k=0}^{N} A_k h_k(t)+s_{N+1}(t) \tag{44}$$

where $h_k(t)$ denotes a desired signal model, such as a chirplet,

$$h_k(t)=\left(\frac{\alpha_k}{\pi}\right)^{\frac{1}{4}} \exp\{-\alpha_k(t-t_k)^2+j[\omega_k+\frac{\beta_k}{2}(t-t_k)](t-t_k)\} \tag{45}$$

which has unit energy, that is,

$$\|h_k(t)\|^2=\int_{-\infty}^{\infty}|h_k(t)|^2\,dt=1 \tag{46}$$

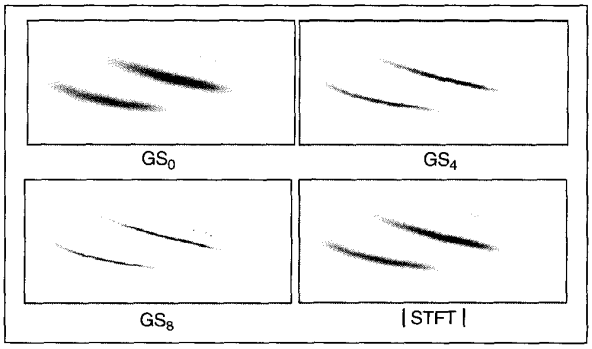

▲ *17. Comparison of GS and STFT-based spectrogram.*

$s_k(t)$ in (44) denotes the residue after the kth approximation. For example,

$$s_0(t)=s(t) \tag{47}$$

$$s_1(t)=s_0(t)-\langle s_0(t),h_0(t)\rangle h_0(t)=s_0(t)-A_0h_0(t) \tag{48}$$

... ...

$$s_{N+1}(t)=s_N(t)-\langle s_N(t),h_N(t)\rangle h_N(t)=s_N(t)-A_Nh_N(t) \tag{49}$$

where the coefficient A_k indicates the signal projection on the elementary function $h_k(t)$. The elementary function $h_k(t)$ is selected such that the residue is minimum, i.e.,

$$\min_{h_k(t)}\|s_{k+1}(t)\|^2=\min_{h_k(t)}\|s_k(t)-\langle s_k(t),h_k(t)\rangle h_k(t)\|^2. \tag{50}$$

It is easy to see that adding (47), (48), and (49) yields (44). Based on (46) and (48), we have

$$\|s_1(t)\|^2 = \|s_0(t)\|^2 - |A_0|^2 \tag{51}$$

$$\|s_2(t)\|^2 = \|s_1(t)\|^2 - |A_1|^2 = \|s_0(t)\|^2 - |A_0|^2 - |A_1|^2 \tag{52}$$

... ...
and finally,

$$\|s(t)\|^2 = \sum_{k=0}^{N} |A_k|^2 + \|s_{N+1}(t)\|^2 . \tag{53}$$

It can be shown that the residue $\|s_{N+1}(t)\|^2$ converges as the number of terms N increases. In real applications, we usually neglect the residue when it is small enough, to rewrite (44) as

$$s(t) = \sum_{k=0}^{\infty} A_k h_k(t) \tag{54}$$

and (53) as

$$\|s(t)\|^2 = \sum_{k=0}^{\infty} |A_k|^2 . \tag{55}$$

Taking the WVD on the both sides of (54) yields

$$WVD_s(t,\omega) = \sum_{k=0} |A_k|^2 WVD_{h_k}(t,\omega) + \sum_{k=0} \sum_{k'=0} A_k (A_{k'})^* WVD_{h_k h_{k'}}(t,\omega) . \tag{56}$$

The first summation represents the set of autoterms, whereas the second indicates the set of crossterms. Because the Wigner-Ville distribution conserves energy (39) and is a using relationship (55), we have the adaptive spectrogram as

$$AD_s(t,\omega) = \sum_{k=0} |A_k|^2 WVD_{h_k}(t,\omega) . \tag{57}$$

Formula (54) is a signal adaptive approximation, which was independently developed by the authors of this article and Mallat et al [36], [41], [43], [45]. When the elementary function $h_k(t)$ has a form (45), we name (57) as a chirplet-based adaptive spectrogram.

The chirplet-based adaptive spectrogram has very high resolution without crossterm interference. Compared to the nonparametric methods, the parametric algorithms are computationally intensive. The key issue of signal adaptive approximation and chirplet-based adaptive spectrogram [73] is the estimation of the optimal elementary function $h_k(t)$ in (50). Usually, they are only suitable for certain types of signals. However, they could perform extremely well if a parametric model indeed fits the analyzed signal [57], [60].

While the STFT and Gabor expansion provide vehicles to map a signal between the time domain and time-frequency domain, the time-dependent spectrum is a powerful tool for understanding the nature of those signals whose power spectra change with time.

Summary

In this article, we briefly introduced the concepts and methods of joint time-frequency analysis. Like the classical Fourier analysis, the mathematical tools of joint time-frequency analysis are also inner product and expansion. Moreover, the joint time-frequency algorithms also fall into two categories: linear and quadratic. While the STFT and Gabor expansion provide vehicles to map a signal between the time domain and time-frequency domain, the time-dependent spectrum is a powerful tool for understanding the nature of those signals whose power spectra change with time. The material presented in this article appears to have reached a level of maturity for real applications [9], [11]-[13], [15], [52], [55], [56], [60], [61].

Note that all methods introduced in this section are mainly designed for signals whose frequency contents change rapidly over time. But their high performance is at the cost of computational complexity. Many applications may start with the STFT-based spectrogram when a signal's frequencies do not change dramatically because the STFT-based spectrogram is simple and easily implemented. When high resolution is a must, the Gabor spectrogram is usually a favorite because it is relatively robust and computationally efficient.

Acknowledgments

The authors wish to express their deep appreciation to Professors Piotr J. Durka, Hans G. Feichtinger, Shidong Li, Flemming Pedersen, and XangGen Xia for their many constructive comments as well as advice. The authors would also like to thank their colleague, Dr. Mahesh Chugani, for his careful reading of manuscripts and valuable suggestions.

Shie Qian is a Senior Research Scientist in the Advanced Signal Processing Department at National Instruments Co. (shie.qian@natinst.com). *Dr. Dapang Chen* is Manager of the Advanced Signal Processing Department at National Instruments Co. (dapang.chen@natinst.com).

References

[1] J.B. Allen and L.R. Rabiner, "A unified approach to short-time Fourier transform analysis and synthesis", *Proc. IEEE*, vol. 65, no. 11, pp. 1558-1564, 1977.

[2] M. Amin, "Time-frequency spectrum analysis and estimation for nonstationary random processes," in *Time-Frequency Signal Analysis: Methods and Applications*, B. Boashash, Ed., pp. 208-232, Australia: Wiley Halsted Press, 1992.

[3] M.J. Bastiaans, "Gabor's expansion of a signal into Gabor elementary signals," *Proc. IEEE*, vol. 68, pp. 538-539, 1980.

[4] M.J. Bastiaans, "A sampling theorem for the complex spectrogram, and Gabor's expansion of a signal in Gaussian elementary signals," *Optical Engineering*, vol. 20, no. 4, pp. 594-598, July/August 1981.

[5] M.J. Bastiaans, "On the sliding-window representation in digital signal processing," *IEEE Trans. Acoust., Speech, Signal Processing*, vol. ASSP-33, no. 4, pp. 868-873, August 1985.

[6] R.G. Baraniuk and D.L. Jones, "A signal-dependent time-frequency representation," *IEEE Trans. Signal Processing*, vol. 41, no. 1, pp. 1589-1602, January 1994.

[7] G.F. Boudreaux-Bartels and T.W. Parks, "Time-varying filtering and signal estimation using Wigner distribution synthesis techniques," *IEEE Trans. Acoust., Speech, Signal Processing*, vol. 34, no. 6, pp. 442- 451, June 1986.

[8] V. Chen, "Radar ambiguity function, time-varying matched filter, and optimal wavelet correlator," *Optical Engineering*, vol. 33, no. 7, pp. 2212-2217, 1994.

[9] V. Chen and S. Qian, "Time-frequency transform vs. Fourier transform for radar imaging," *Proc. IEEE-SP International Symposium on Time-Frequency and Time-Scale Analysis*, Paris, France, pp. 389-392, June 1996.

[10] V. Chen, "CFAR detection and extraction of unknown signal in noise with time-frequency Gabor transform," *Proc. SPIE on Wavelet Applications*, vol. 2762, pp. 285-294, April 1996.

[11] V. Chen, "Applications of time-frequency processing to radar imaging," *Optical Engineering*, vol. 36, no. 4, pp. 1152-1161, Apr. 1997.

[12] V. Chen, "Time-frequency-based ISAR image formation technique," *Proc. SPIE on Algorithms for Synthetic Aperture Radar Imagery*, vol. 3070, pp. 43-54, April 1997.

[13] V. Chen and S. Qian, "Joint time-frequency transform for radar range-doppler imaging," *IEEE Trans. Aerosp. Electron. Syst.*, vol. 34, no. 2, pp. 486-499, April 1998.

[14] H. Choi and W.J. Williams, "Improved time-frequency representation of multicomponent signals using exponential kernels," *IEEE Trans. Acoust., Speech, Signal Processing*, vol. 37, no. 6, pp. 862-871, June 1989.

[15] M. Chugani, "Feature analysis of Doppler ultrasound signals obtained from mammalian arteries," Ph.D. Thesis, Rensselaer Polytechnic Institute, August 1996.

[16] T. Claasen and W. Mecklenbrauker, "The Wigner-distribution – a tool for time-frequency signal analysis – Part I: Continuous-time signals, Part II: Discrete – time signals, Part III: Relations with other time-frequency signal transformations," *Philips J. Res.*, vol. 35, no. 3, pp. 217-250, 1980.

[17] L. Cohen, "Generalized phase-space distribution functions," *J. Math. Phys.*, vol. 7, pp. 781-806, 1966.

[18] L. Cohen, "Time-frequency distribution–a review," *Proc. IEEE*, vol. 77, no. 7, pp. 941-981, July 1989.

[19] L. Cohen, *Time-Frequency Analysis*, Englewood Cliffs, NJ: Prentice Hall, 1995.

[20] R.E. Crochiere and L.R. Rabiner, *Multirate Digital Signal Processing*, Englewood Cliffs, NJ: Prentice-Hall, 1983.

[21] I. Daubechies, "The wavelet transform, time-frequency localization, and signal analysis," *IEEE Trans. Inform. Theory*, pp. 961-1005, September 1990.

[22] P.D. Einziger, "Gabor expansion of an aperture field in exponential elementary beams," *IEE Electron. Lett.*, vol. 24, pp. 665-666, 1988.

[23] S. Farkash and S. Raz, "Time-variant filtering via the Gabor expansion," *Signal Processing V: Theories and Applications*, pp. 509-512, New York: Elsevier, 1990.

[24] H. Feichtinger and T. Stromas, *Gabor Analysis and Algorithms: Theory and Applications*, Birkhauser, 1998.

[25] B. Friedlander and B. Porat, "Detection of transient signal by the Gabor representation," *IEEE Trans. Acoust., Speech, Signal Processing*, vol. 37, no. 2, pp. 169-180, February 1989.

[26] D. Gabor, "Theory of communication," *J. IEE*, vol. 93, no. III, pp. 429-457, November 1946.

[27] F. Hlawatsch and W. Krattenthaler, "Bilinear signal synthesis," *IEEE Trans. Signal Processing*, vol. 40, no. 2, pp. 352-363, February 1992.

[28] F. Hlawatsch and G.F. Boudreaux-Bartels, "Linear and quadratic time-frequency signal representations," *IEEE Signal Processing Magazine*, vol. 9, no. 2, pp. 21-67, March 1992.

[29] A.J.E.M. Janssen, "Gabor representation of generalized functions," *J. Math. Anal. Appl.*, vol. 38, pp. 377-394, 1981.

[30] A.J.E.M. Janssen, "Optimality property of the Gaussian window spectrogram," *IEEE Trans. Signal Processing*, vol. 39, no. 1, pp. 202-204, January 1991.

[31] A.J.E.M. Janssen, "Duality and biorthogonality for Weyl-Heisenberg frame," to appear in *J. Fourier Anal. Appl.*

[32] R. Koenig, H.K. Dunn, and L.Y. Lacy, "The sound spectrograph," *J. Acoust. Soc. Amer.*, vol. 18, pp. 19-49, 1946.

[33] S. Li, "A general theory of discrete Gabor expansion," *Proc. SPIE'94 Mathematical Imaging: Wavelet Applications*, San Diego, CA, July 1994.

[34] S. Li and D.M. Healy Jr. "A parametric class of discrete Gabor expansions," *IEEE Trans. Signal Processing*, vol. 44, no. 2, pp. 201-211, February 1996.

[35] Y. Lu and J.M. Morris, "Gabor Expansion for Echo Cancellation," *Signal Processing Magazine*, March 1999.

[36] S. Mallat and Z. Zhang, "Matching pursuit with time-frequency dictionaries," *IEEE Trans. Signal Processing*, vol. 41, no. 12, pp. 3397-3415, December 1993.

[37] J.M. Morris and Y. Lu, "Discrete Gabor expansion of discrete-time signals in l2(Z) via frame theory", *IEEE Signal Processing Magazine*, vol. 40, no. 2 pp.155-181, March. 1994.

[38] C.H. Page, "Instantaneous power spectrum," *J. Appl. Phys.*, vol. 23, pp. 103-106, 1952.

[39] F. Pedersen, "The Gabor-expansion-based time-frequency spectra," *Proc. ICASSP'98*, Seattle, WA, May 1998.

[40] M.R. Protnoff, "Time-frequency representation of digital signal and systems based on short-time Fourier analysis," *IEEE Trans. Acoust., Speech, Signal Processing*, vol. 28, no. 1, pp. 55-69, February 1980.

[41] S. Qian, D. Chen, and K. Chen, "Signal approximation via data-adaptive normalized Gaussian functions and its applications for speech processing," *Proc. ICASSP'92*, San Francisco, CA, pp. 141-144, March 1992.

[42] S. Qian and J.M. Morris, "Wigner distribution decomposition and cross-term deleted representation," *Signal Processing*, vol. 25, no. 2, pp. 125-144, May 1992.

[43] S. Qian and D. Chen, "Signal representation in adaptive Gaussian functions and adaptive spectrogram," *Proc. The 27th Annual Conference on Information Sciences and Systems*, pp. 59-65, Baltimore, MD, March 1993.

[44] S. Qian and D. Chen, "Discrete Gabor transform," *IEEE Trans. Signal Processing*, vol. 41, no. 7, pp. 2429-2439, July 1993.

[45] S. Qian and D. Chen, "Signal representation using adaptive normalized Gaussian functions," *Signal Processing*, vol. 36, no. 1, pp. 1-11, March 1994.

[46] S. Qian and D. Chen, "Decomposition of the Wigner-Ville distribution and time-frequency distribution series" *IEEE Trans. Signal Processing*, vol. 42, no. 10, pp. 2836-2841, October 1994.

[47] S. Qian and D. Chen, *Joint Time-Frequency Analysis*, Englewood Cliffs, NJ: Prentice-Hall, 1996.

[48] S. Qiu and H.G. Feichtinger, "Discrete Gabor structure and optimal representation," *IEEE Trans. Signal Processing*, vol. 43, no. 10, pp. 2258-2268, October 1995.

[49] W. Rihaczek, "Signal energy distribution in time and frequency," *IEEE Trans. Inst. Radio Engineers*, vol. IT-14, pp. 369-374, 1968.

[50] M. Savic, M. Chugani, Z. Macek, M. Tang, and A. Husain, "Detection of stenotic plaque in arteries," *Proc. 15th Annual International Conference of the IEEE Engineering in Medicine and Biology Society*, San Diego, CA, pp. 317-318, October 1993.

[51] M. Savic, M. Chugani, K. Peabody, A. Husain, M. Tang, and Z. Macek, "Digital signal processing aids cholesterol plaque detection," *Proc. ICASSP'95*, Detroit, MI, pp. 1173-1176, May 1995.

[52] R.J. Sclabassi, M. Sun, D.N. Krieger, P. Jasiukaitis, and M.S. Scher, "Time-frequency analysis of the EEG signal," in *Proc. ISSP'90, Signal Processing, Theories, Implementations and Applications*, Gold Coast, Australia, pp. 935-942, 1990.

[53] R.J. Sclabassi, M. Sun, D.N. Krieger, P. Jasiukaitis, and M.S. Scher, "Time-frequency domain problems in the neurosciences," in *Time-Frequency Signal Analysis: Methods and Applications*, B. Boashash, Ed., Longman-Cheshire, England: Wiley Halsted Press, pp. 498-519, 1992.

[54] G. Strang and T.Q. Nguyen, *Wavelet and Filter Banks*. Wellesley, MA: Wellesley-Cambridge Press, 1995.

[55] M. Sun, S. Qian, X. Yan, S. Baumann, X.-G. Xia, R. Dehl, N. Ryan, and R. Sclabassi, "Localizing functional activity in the brain through time-frequency analysis and synthesis of the EEG," *Proc. IEEE*, vol. 85, no. 9, pp. 1302-1311, November 1996.

[56] M. Sun, M.L. Scheuer, S. Qian, S.B. Baumann, P.D. Adelson, and R.J. Sclabassi, "Time-frequency analysis of high-frequency activity at the start of epileptic seizures," *Proc. IEEE EMBC'97*, Chicago, IL, October 1997.

[57] L. Trintinalia and H. Ling, "Joint time-frequency ISAR using adaptive processing," *IEEE Trans. Antennas Propagat.*, vol. 45, no. 2, pp. 221-227, February 1997.

[58] P.P. Vaidyanathan, *Multirate Systems and Filter Banks*, Englewood Cliffs, NJ: Prentice Hall, 1993.

[59] J. Ville, "Thovrie et applications de la notion de signal analylique," (in French) *Câbles et Transmission*, vol. 2, pp. 61-74, 1948.

[60] J. Wang and J. Zhou, "Chirplet-based signal approximation for strong earthquake ground motion model," this issue, pp. 94.

[61] Y.Wang, H.Ling, and V.C.Chen, "ISAR motion compensation via adaptive joint time-frequency technique", *IEEE Trans. AES-34*, to appear.

[62] T.P. Wang, M. Sun, C.C. Li and A.H. Vagnucci, "Classification of abnormal cortisol patterns by features from Wigner spectra," in *Proc. 10th International Conference on Pattern Recognition*, Atlantic City, NJ, pp. 228-230, June 1990.

[63] J. Wexler and S. Raz, "Discrete Gabor expansions," *Signal Processing*, vol. 21, no. 3, pp. 207-221, November 1990.

[64] E.P. Wigner, "On the quantum correction for thermodynamic equilibrium," *Phys. Rev.*, vol. 40, pp. 749, 1932.

[65] C. Wilcox, "The synthesis problem for radar ambiguity functions," *Tech. Summary Rep. 157*, Math. Res. Center, University of Wisconsin at Madison, April 1960.

[66] W.J. Williams, "Reduced interference distributions: biological applications and interpretations," *Proc. IEEE*, vol. 84, no. 9, pp. 1264-1280, September 1996.

[67] D. Wu and J.M. Morris, "Time-frequency representations using a radial Butterworth kernel," *Proc. IEEE-SP International Symposium on Time-Frequency and Time-Scale Analysis*, pp. 60-63, Philadelphia, PA, October 1994.

[68] D. Wu, "Time-frequency signal analysis via Cohen's class of distributions and implementation algorithms," Ph.D. Thesis, University of Maryland at Baltimore, May 1998.

[69] X.-G. Xia and S. Qian, "An iterative algorithm for time-varying filtering in the discrete Gabor transform domain," *IEEE Trans. on Signal Processing*, to be published.

[70] X.-G. Xia, "System identification using chirp signals and time-varying filters in the joint time-frequency domain," *IEEE Trans. Signal Processing*, vol. 45, no. 8, pp. 2072-2084, August 1997.

[71] X.-G. Xia, "A quantitative analysis of SNR in the short-time Fourier transform domain for multicomponent signals," *IEEE Trans. Signal Processing*, vol. 46, pp. 200-203, January 1998.

[72] J. Yao, "Complete Gabor transformation for signal representation," *IEEE Trans. Image Processing*, vol. 2, pp. 152-159, April 1993.

[73] Q. Yin, Z. Ni, S. Qian, and D. Chen, "Adaptive oriented orthogonal projective decomposition," *J. Electron.* (Chinese), vol. 25, no. 4, pp. 52-58, April 1997.

[74] Y. Zhao, L.E. Atlas, and R.J. Marks, "The use of cone-shaped kernels for generalized time-frequency representations of nonstationary signals," *IEEE Trans. Acoust., Speech, Signal Processing*, vol. 38, no. 7, pp. 1084-1091, July 1990.